Local Structure around Iron(III) Ion in Lamprey Hemoglobin

Tsutomu KURISAKI[1)], Hisao YAMASHIGE[1)], Youichi YAZAWA[2)], and Hisanobu WAKITA[1)]

(Received December 19, 2009)

Abstract

X-ray absorption near-edge structure (XANES) measurements at Fe K absorption edge were performed for iron(III)-tetrakis(*p*-sulfonatophenyl)porphyrin (FeTSPP) and Lamprey Hemoglobin (L-Hb). The spectral shapes differ in the Fe K XANES spectra. The electronic states of FeTSPP and L-Hb were also estimated by the analysis using discrete variational (DV)-Xα molecular orbital (MO) method. The combination of XANES spectra and DV-Xα MO calculation shows that the Fe ion in L-Hb takes the oxidation state of divalent and is linked with one oxygen molecule.

1. Introduction

X-ray absorption near-edge structure (XANES) is a powerful tool for investigating electronic and steric structure around an absorption atom, and has extensively been applied for heme irons in heme proteins, for example, peroxidases including horseradish peroxidase,[1-3] cytochrome-c peroxidase, [1, 4] lacto-peroxidase, [5] chloroperoxidase,[6] and lignin peroxidase. [7, 8]

Hemoglobin (Hb) is also a kind of heme protein, which is particularly in blood of vertebrates, and serves as a transport protein not only of O_2, but also of CO_2 and H^+. [9-11] The chemical state and interaction between O_2 molecules and active center Fe ions in Hb, especially human Hb, have been discussed using various spectroscopic techniques, [12-19] including XANES near the Fe absorption edge. [20] Human Hb consists of four subunit proteins which are divided into two types of polypeptide chain, α and *β* chains. This means that there are at least two types of Fe ion, the coordination structure of which differs. In the point, the studies described above should provide the average structure of two Fe species. Accordingly, the electronic and steric structure around the Fe ion in human Hb have been insufficiently understood.

Lamprey belongs to cyclostomata in fishes, which has the most primitive Hb in vertebrates. Lamprey Hb consists of one type of polypeptide chain unlike human Hb. Lamprey Hb which was crystallized by isolation and refinement (L-Hb) is triclinic crystal, three-dimension structure of which is very similar to that of human Hb *β* chain (Fig. 1). [21] Therefore, L-Hb instead of human Hb enables to obtain more clear information on electronic and steric structure around the Fe ion by means of Fe K XANES.

This paper is intended to report the electronic and local structure of Fe ion in L-Hb, especially with an O_2 molecule coordination, using XANES near Fe K absorption edge. The experimental XANES spectra are theoretically analyzed using a discrete variational (DV)-Xα molecular orbital (MO) method as an electronic state calculation method.

2. Experimental

2-1. Materials

Lamprey Hb was purified from river lamprey *Lampetra japonica* using DEAE-Toyopearl column chromatography. [22] The aqueous solution of L-Hb was prepared to ca. 30 – 40 mg/ml. Tetrakis(*p*-sulfonatophenyl)porphyriniron(III) (FeTSPP) was

1) Department of Chemistry, Faculty of Science, Fukuoka University, 8-19-1 Nanakuma, Jonan-ku, Fukuoka, 814-0180, Japan

2) Asahikawa Campus, Hokkaido University of Education, Asahikawa, 070-8621 Japan

Fig. 1 Comparing of the steric structures of β chain in L-Hb and human Hb. Structures of L-Hb and human Hb indicate red and green colors, and heme indicates stick model.

synthesized as a reference sample for L-Hb according to the procedure as reported by Fleischer et al..[23]

2-2. XANES

The Fe K XANES measurements, which were performed in the X-ray fluorescence yield mode using Lytle detector, were made at BL7C with a two Si (111) crystal monochromator in the Photon Factory (PF), KEK, Tsukuba, Japan. During the measurements, the PF operated in the multi-bunch mode, the strage-ring energy was 2.5 GeV and the current decayed from 400 to 300 mA. The measurement of the aqueous solution of L-Hb was carried out, while it was cooled by the ice. The measurement of the aqueous solution of FeTSPP was carried out at the room temperature. The spectral acquisition range was 7100 eV to 7150 eV, counting at intervals of 0.5 eV. The dwell time of a data point was 4 sec for L-Hb and 3 sec for FeTSPP. Photon energy was calibrated at 8979.0 eV of Cu K-edge of Cu foil.

2-3. Calculation

The structural models of L-Hb and FeTSPP were constructed from single-crystal structure data of Tetraphenylporphyrin, [24] and were optimized using the Amsterdam density functional (ADF) program package. [25-27] Computational details of the DV-Xα MO method have been described elsewhere. [28] Figure 2 shows the structural models of L-Hb and FeTSPP for DV-Xα MO calculations. The calculations for both models were carried out using the numerical atomic orbitals of 1s to 5p for Fe, 1s to 3d for S, 1s to 3p for N and O, 1s to 2p for C, and 1s for H as basis sets. The DV numerical integration was made at 1000 points per atom. Convergence of self-consistent-field iterations was set to 0.001 electrons which means

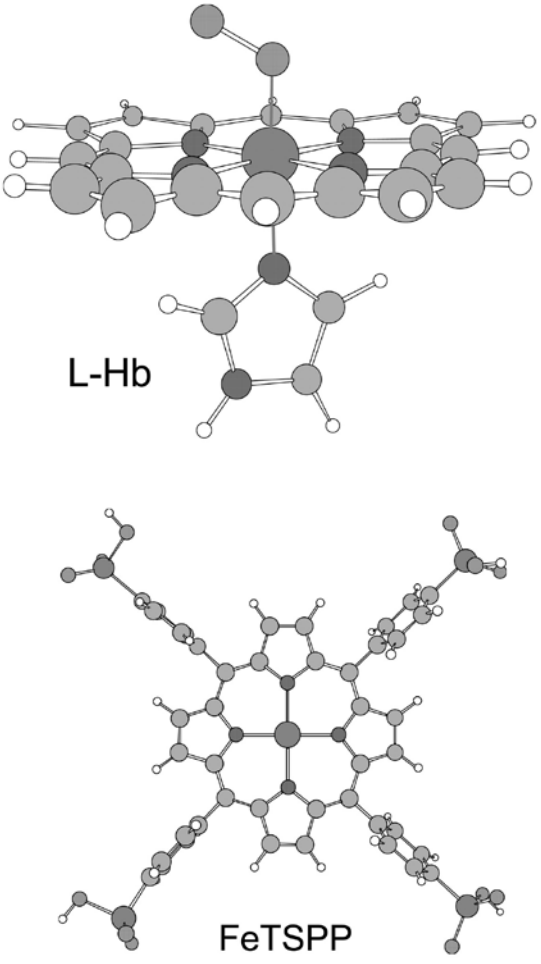

Fig. 2 Structural models of FeTSPP and L-Hb for DV-Xα calculations. These models were optimized in advance using the ADF program package.

the difference before and after an iteration. Densities of states (DOSs) and electron transition probabilities (ETPs) were calculated using electron-state data of MOs obtained by DV-Xα MO calculations.

3. Results and Discussion

Figure 3 shows experimental Fe K XANES spectra (solid line) in the range of 7100 eV to 7150 eV for FeTSPP and L-Hb. Characters of A to E represent remarkable features around 7114, 7123, 7130, 7135, and 7140 eV in the spectrum for L-Hb, respectively, which is compared with that for FeTSPP at the points of the features to discuss the coordination and electronic structure of each Fe ion. Pre-edge peak A, in general, is assigned to the electron transition from Fe 1s orbital to an Fe 3d orbital, and indicates the oxidation state of Fe. [29-36] Accordingly, the oxidation states of Fe in L-Hb and FeTSPP would be assigned to two and three in positive, respectively. Therefore, an O_2 molecule is linked by coordination to the active center Fe(II) ion in L-Hb.

The calculated ETPs (bars) for FeTSPP and L-Hb models in Fig. 2 are shown in Figs. 4 and 5 along with the corresponding experimental Fe K XANES spectrum (solid line) in the range of 7100 eV to 7150 eV, respectively. The theoretical curve (broken line) was obtained by convoluting ETPs using a Gaussian function with 2.0 eV of FWHM. The labeled **a-e** on ETPs in both Figs. 4 and 5 are correspondent with the labeled A-E as defined in Fig. 3, respectively. For FeTSPP in Fig. 4, the MO for ETP **a** consists of Fe 3d orbital, and all the MOs for ETP **b-d** consist of Fe 4p, N 3p, and C 2p orbitals. For L-Hb in Fig. 5, on the other hand, the MO for ETP **a** consists of an Fe 3d orbital, and all the MOs for ETP **b-d** consist of Fe 5p, Fe 4p, N 3p, and O 3p orbitals. The differences of intensity for peak B, C, and E between FeTSPP and L-Hb originate from the intensities and position of ETPs b, c, and e as can be seen from the comparison of the theoretical curve between FeTSPP and L-Hb. The lower energy shift for feature D of L-Hb than that of FeTSPP is connected with the position of ETP c of L-Hb. These results suggest that the O 3p orbital of O_2 molecule and the N 3p orbital of histidine residue concern the spectral feature of Fe K XANES for L-Hb. However, the influence of the O and N 3p orbital on the experimental spectral feature of L-Hb can be seen by PDOS for 3p orbitals of O atoms proximal

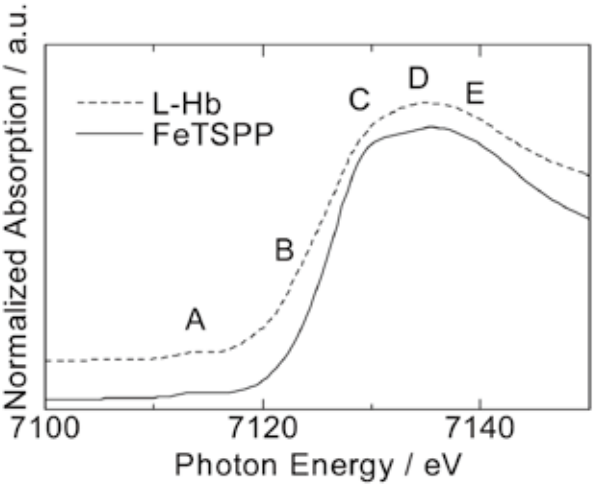

Fig. 3 Observed Fe K XANES spectra of FeTSPP (solid line) and L-Hb (broken line).

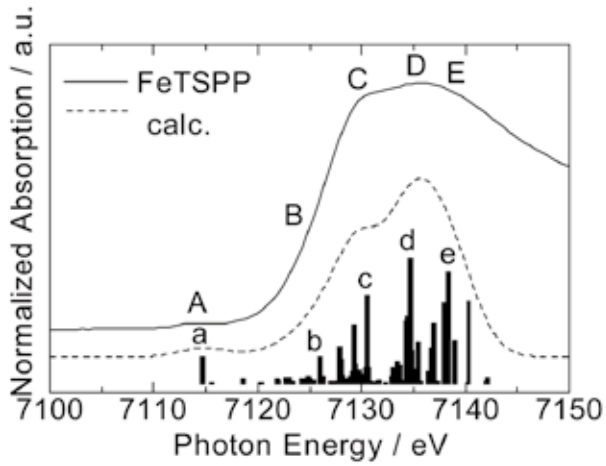

Fig. 4 Calculated ETPs (bars), gaussian convoluted curve, and experimental Fe K XANES spectra (solid line) for FeTSPP

(denoted O_{prox}, solid line) and distal (denoted O_{dist}, broken line) to the Fe(II) ion, and of the N atom calculated by DV-Xα MO method in Fig.6. Main peak in each PDOS appears at 7135 eV for O_{prox} 3p orbital, at 7126 eV for O_{dist} 3p orbital, and at 7124 eV for N 3p orbital. Therefore, it is considered that O_{prox} 3p and N 3p orbitals, and O_{dist} 3p and N 3p orbitals mainly affect features D and B, respectively.

The influence of O_2 molecules coordinating to the Fe(II) in L-Hb on the spectral feature of Fe K XANES has been investigated from the calculated ETPs (bars) for L-Hb and deoxygenated L-Hb ($L\text{-}Hb_{deoxy}$) models as shown in Fig. 7, where the

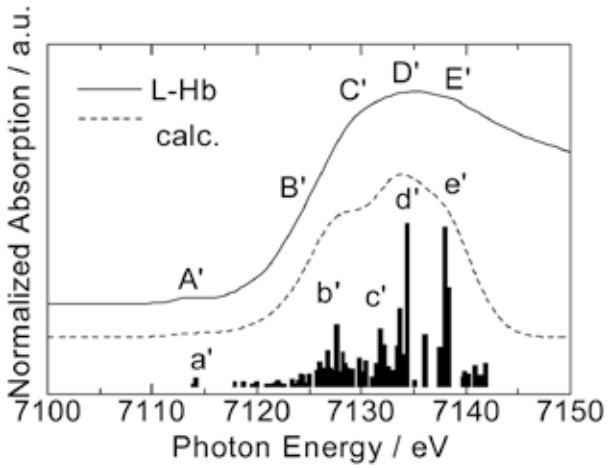

Fig. 5 Calculated ETPs (bars), gaussian convoluted curve, and experimental Fe K XANES spectra (solid line) for L-Hb.

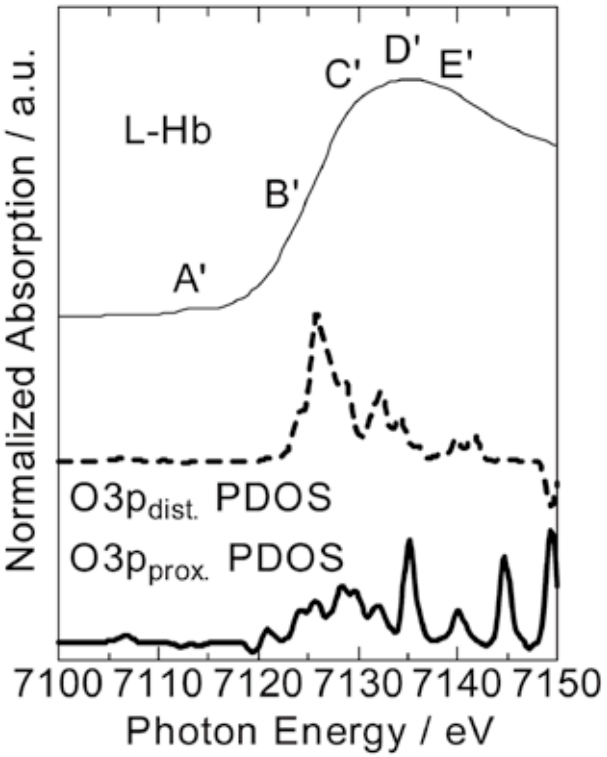

Fig. 6 Calculated O 3p$_{prox}$ PDOS (bold solid line), O 3p$_{dist}$ PDOS (bold broken line) and experimental Fe K XANES spectrum (solid line) for L-Hb.

theoretical curve (solid line) was obtained by convoluting ETPs using a Gaussian function with 2.0 eV of FWHM. Electron transition probabilities in L-Hb$_{deoxy}$, which two arrows indicate at 7126 eV and 7134 eV, are lower intensity than that in L-Hb. The result of this simulation indicates that an O_2 molecule which is linking by coordination to Fe(II) ion in L-Hb affects features B and D as shown in Fig. 6. Therefore, features B and D on Fe K XANES spectrum for L-Hb enable to obtain information on chemical interaction between an O_2 molecule and the Fe(II) ion in L-Hb in the process of the transport.

4. Conclusion

Iron K XANES spectrum for L-Hb is first data for Hb consisting of one type of polypeptide chain, which is similar in steric structure to human Hb β chain. The spectrum has indicated that the oxidation state of the Fe ion linking with O_2 molecule becomes divalent, and that the O_2 molecule and N atom of the histidine residue affect the features around 7135, 7126, and 7124 eV by the electronic state analysis and the XANES simulation using the DV-Xα MO method. The spectrum of L-Hb will allow to discuss the change of the oxidation state of Fe ion on the process of the transport of an O_2 molecule, and to provide useful information on the electronic state and local structure of Fe ion in human Hb and other heme units.

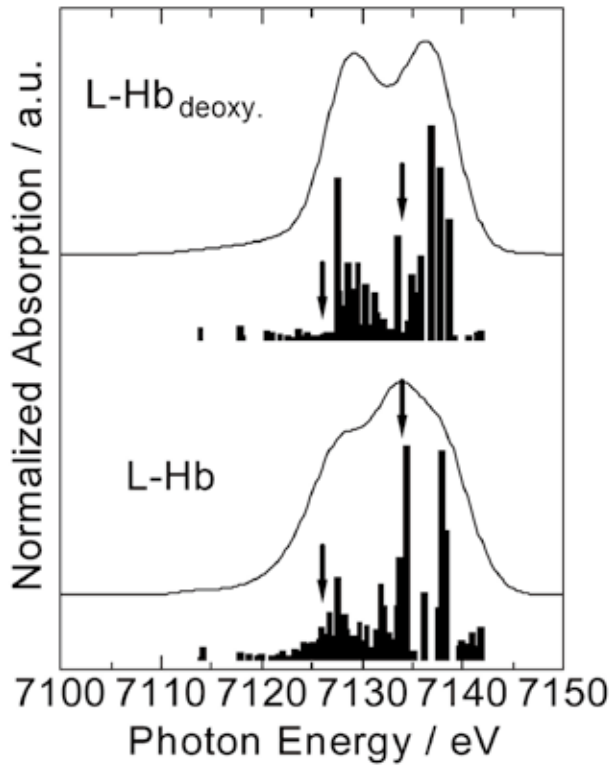

Fig. 7 Calculated ETPs (bars) and gaussian convoluted curves (solid line) for L-Hb and L-Hb$_{deoxy}$. are shown at lower and upper sides, respectively.

References

[1] Chance B, Powers L, Ching Y, Poulos TL, Schonbaum G, Yamazaki L, Paul KG. *Arch. Biochem. Biophys.* 1984; **235**: 596.

[2] Chang CS, Yamazaki I, Sinclair R, Khalid S, Powers L. *Biochemistry* 1993; **32**: 923.

[3] Hahn JP, McMurray T, Renner M, Grazynski LL, Eble K, Davis I, Balch A, Groves J, Dawson J, Hodgson K. *J. Biol. Chem.* 1983; 258.

[4] Chance M, Parkhurst L, Powers L, Chance B. *J. Biol. Chem.* 1986; **261**: 5689.

[5] Chang CS, Sinclair R, Khalid S, Yamazaki I, Nakamura S, Powers L. *Biochemistry* 1993; **32**: 2780.

[6] Cramer S, Dawson J, Hodgson K, Hager L. *J. Am. Chem. Soc.* 1978; **100**: 7282.

[7] Sinclair R, Powers L, Bumpus J, Albo A, Brock B. *Biochemistry* 1992; **31**: 4892.

[8] Sinclair R, Copeland B, Yamazaki Y, Powers L. *Biochemistry* 1995; **34**: 13176.

[9] Monod J, Wyman J, Changeux JP. *J. Mol. Biol.* 1965; **12**: 88.

[10] Perutz MF. *Quart. Rev. Biophys.* 1989; **22**: 139.

[11] Uoroki M, Yazawa Y. *Journal of Hokkaido University of Education* (*Natural Science*) 2001; **51**: 61.

[12] Amiconi G, Santucci R, Coletta M, Castellano AC, Giovannelli A, Ariccia MD, Longa SD, Barteri M, Burattini E, Bianconi A. *Biochemistry* 1989; **28**: 8547.

[13] Bianconi A, Castellano AC, Giovannelli A, Ariccia MD, Burattini E, Durham PJ, Giacometti GM. *Eur. Biophys. J.* 1986; **14**: 7.

[14] Choc MG, Caughey WS. *J. Biol. Chem.* 1981; **256**: 1831.

[15] Durham P, Bianconi A, Castellano AC, Giovannelli A, Hasnain SS, Incoccia L, Morante S, Pendry JB. *EMBO J.* 1983; **2**: 1441.

[16] Antri SEl, Zentz C, Alpert B. *Eur. J. Biochem.* 1989; **179**: 165.

[17] Makinen MW, Houtchens RA, Caughey WS. *Proc. Natl. Acad. Sci. U.S.A.* 1979; **76**: 6042.

[18] Pin S, Valat P, Cortes R, Michalowicz A, Alper B. *Biophys. J.* 1985; **48**: 997.

[19] Sugita Y, Nagai M, Yoneyama Y. *J. Biol. Chem.* 1971; **246**: 383.

[20] Zentz C, Antri SE, Pin S, Cortes R, Massat A, Simon M, Alpert B. *Biochemistry* 1991; **30**: 2804.

[21] Kamidochi-Seki M, Yao M, Tanaka I, Nakayama T, Yazawa T. *Reports of the Taisetsuzan Institute of Science* (*Hokkaido University of Education*) 2002; **36**: 67.

[22] Yazawa Y, Kitamura H, Taura T, Higashihara M, Hirose T, Kamidochi-Seki M, Tanaka I. *Journal of Hokkaido University of Education* (*Natural Science)* 2000; **50**: 1.

[23] Fleischer EB, Palmer JM, Srivastava TS, Chatterjee A. *J. Am. Chem. Soc.* 1971; **93**: 3162.

[24] Song B, Swenson DC, Goff HM. *Acta Cryst. C*54 1998; IUC9800058.

[25] Velde G, Bickelhaupt FM, Gisbergen SJA, Guerra CF, Baerends EJ, Snijders JG, Ziegler T. *J. Comput. Chem.* 2001; **22**: 931.

[26] Guerra CF, Snijders JG, Velde G, Baerends EJ. *Theor. Chem. Acc.* 1998; **99**: 391.

[27] ADF2004.01, SCM, Theoretical Chemistry, Vrije Universiteit, Amsterdam, The Netherlands, http://www.scm.com.

[28] Adachi H, Tsukada M, Satoko C. *J. Phys. Soc. Jpn.* 1978; **45**: 875.

[29] Brown GE, Keefer KD, Fenn PM, *Prog. Geol. Soc. Am. Ann. Manage.* 1978; **10**: 373.

[30] Calas G, Petiau J. *Bull. Mineral.* 1983; **106**: 33.

[31] Calas G, Petiau J. *Solid State Commun.* 1983; **48**: 625.

[32] Brown GE, Farges F, Calas G. in *Structure Dynamics and Properties of Silicate Melts,* edited by Stebbins JF, Dingwell DB, McMillan PF, Vol. 32, p 317. The American Society of America, Washington, 1995.

[33] Delaney JS, Dyar MD, Sutton SR, Bajt S. *Geology* 1998; **26**: 139.

[34] Wilke M, Farges F, Behrens H, Burkhard D. *Eur. J. Mineral.* 1999; **11**: 244.

[35] Mosbah MB, Simionovici AS, Metrich N, Duraud JP, Massare D, Dillmann P. *J. Non-Cryst. Solids* 2001; **288**: 103.

[36] Galoisy L, Calas G, Arrio MA, *Chem. Geol.* 2001; **174**: 307.